JACS
JOURNAL OF THE AMERICAN CHEMICAL SOCIETY

COMMUNICATION

pubs.acs.org/JACS

Layer-by-Layer Processing and Optical Properties of Core/Alloy Nanostructures

Peter N. Njoki,[†] Wenjie Wu,[†] Hui Zhao,[‡] Lukas Hutter,[†] Eric A. Schiff,[‡] and Mathew M. Maye*[,†]

[†]Department of Chemistry and [‡]Department of Physics, Syracuse University, Syracuse, New York 13244, United States

Supporting Information

ABSTRACT: A novel hydrothermal layer-by-layer processing method for the fabrication of core/alloy nanoparticles with highly tunable surface plasmon resonance is described. For a model system of Au/Au_xAg_{1-x}, the processing temperature, alloy composition, and alloy thickness resulted in unique and tailorable plasmonic signatures. The discrete dipole approximation and selective alloy etching were used to correlate this optical response with the particle morphology and alloy phase ultrastructure.

Postsynthetic processing of nanomaterials may allow researchers to obtain specific properties, morphologies, or phase regimes that are not accessible by simple synthesis alone.[1−10] Emerging techniques take advantage of the diffusion or interdiffusion of impurities such as dopants, defects, or atoms at nanointerfaces, which even at modest temperatures have profound effects for confined nanosystems.[1,2] These effects and the resulting changes to the microstructure, lattice type, and spacing are emerging examples of the Kirkendall effect, where, in addition to redox potential, atomic and defect diffusion at the nanoparticle (NP) interface and interior is key.[2−6] Examples of this approach to alter the catalytic, optical, or morphological properties have recently been demonstrated. For example, the use of galvanic reactions at the NP interface has proven to be especially interesting.[7−10] Through the use of sacrificial palladium or silver nanocubes, hollow gold shells or cubic gold cages can be fabricated, and this process can be followed in situ by monitoring the rich plasmonic behavior.[6−10] Another galvanic development is the ability for researchers to alter the optical and catalytic properties via reversible ion-exchange reactions in quantum-dot and quantum-rod superlattices.[3−5] A number of theoretical descriptions have also begun to investigate the role that nanoscale interfacial energies may play in alloy formation.[2,12] For example, alloy interdiffusion is expected to be thermodynamically and kinetically favorable,[2a] and nanoalloys also may be highly stable, largely as a result of relieved interfacial energies.[2b]

In the present system, we explored the use of high-temperature processing to promote alloy-shell formation on a presynthesized NP. The use of high temperature allows for alloy interdiffusion into the NP core, which results in fine control of the shell thickness and alloy composition. For temperature control in an aqueous system, we explored a novel hydrothermal layer-by-layer processing method[11] to fabricate a binary Au/Au_xAg_{1-x} core/alloy system. The Au_xAg_{1-x} system was chosen as a model to explore this approach in large part because of the constituents' miscible binary phase diagram and rich plasmonic behavior.[2−6,9,10,12,14−19]

Figure 1a shows an illustration of our approach. The presynthesized AuNPs were combined with known feed ratios of the alloying components, which in this proof-of-principle study were $[AuBr_4]^-$ and $AgNO_3$. The $[AuBr_4]^-$ complex was chosen in order to have similar redox potentials between the precursors and the Au^0 NP interface ($E° \approx 0.858$ V). The feed ratio, $r = ([Ag^+] + [AuBr_4]^-)/[AuNP]$, was limited to that required for growth of a shell with a thickness (t_S) of only 0.25−0.5 nm. This process was then repeated for n layers. To promote reduction as well as alloy annealing, we employed a novel hydrothermal temperature (T_H) processing method exploiting automated microwave irradiation (MWI) for rapid and controllable dielectric heating.[11,13,14a−14c] The use of a synthetic MW reactor for dynamic MWI facilitates fine control of the heating rate, cooling rates, and processing temperature as well as in situ monitoring of the reaction temperature (Figure 1b) and pressure (Figure 1c), as reported by Strouse,[13] El-Shall,[14a−c] and our previous work.[11]

We began with an aqueous dispersion of AuNP cores (core diameter (d_C) = 15.4 ± 0.7 nm) and deposited shells of Au_xAg_{1-x} alloys with x = 0.0, 0.15, 0.50, 0.85, and 1.0 and controlled t_S. Processing at T_H = 120 or 160 °C produced a highly controllable and unique optical surface plasmon resonance (SPR) as a function of x, t_S, and T_H. The SPR of a core/shell nanomaterial is derived from the size, shape, structure, composition, and surrounding medium of the nanostructure,[15−19] thus making Au/Au_xAg_{1-x} an attractive test case. To follow these optical and morphology changes, we employed UV−vis spectrophotometry (UV−vis) and transmission electron microscopy (TEM). Figure 2 shows a representative set of UV−vis and TEM results for the Au/Au_xAg_{1-x} system at T_H = 120 °C and x = (a) 0.15, (b) 0.50, and (c) 0.85. For example, at x = 0.15 (Figure 2a), we observed a systematic blue shift in λ_{SPR} from the value for AuNPs (520 nm) to 490 nm at n = 3 and a broad SPR further shifted to 405 nm at n = 7. For UV−vis of NPs with n = 1−10 layers, see Figures S1 and S2 in the Supporting Information. Such a blue shift of the SPR is indicative of an increasingly Ag-rich nanostructure.[15,20] The corresponding TEM results for n = 3 and 7 are shown in Figure 2a. Two observations can be made. First, the overall morphology of the core/alloy NPs remained largely unchanged (e.g., spherical), and second, an increase in the core + shell diameter (d_{C+S} = 18.1 ± 1.4 and 21.2 ± 2.0 nm) was observed.

Received: January 22, 2011
Published: March 23, 2011

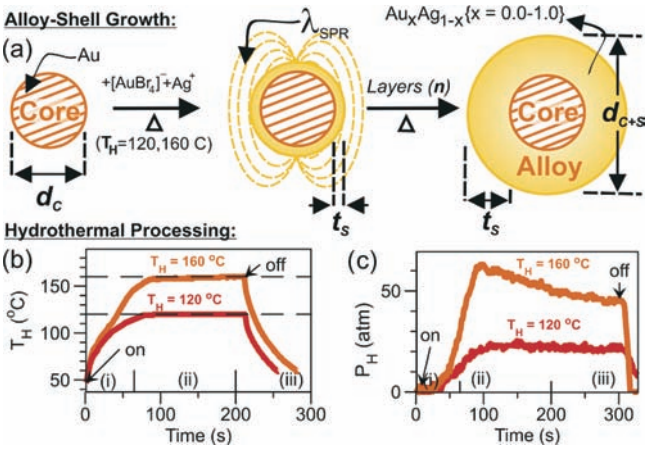

Figure 1. (a) Schematic illustration of the synthesis procedures and core/alloy NP growth. (b, c) In situ (b) temperature and (c) pressure profiles measured during alloy deposition at T_H = 120 and 160 °C.

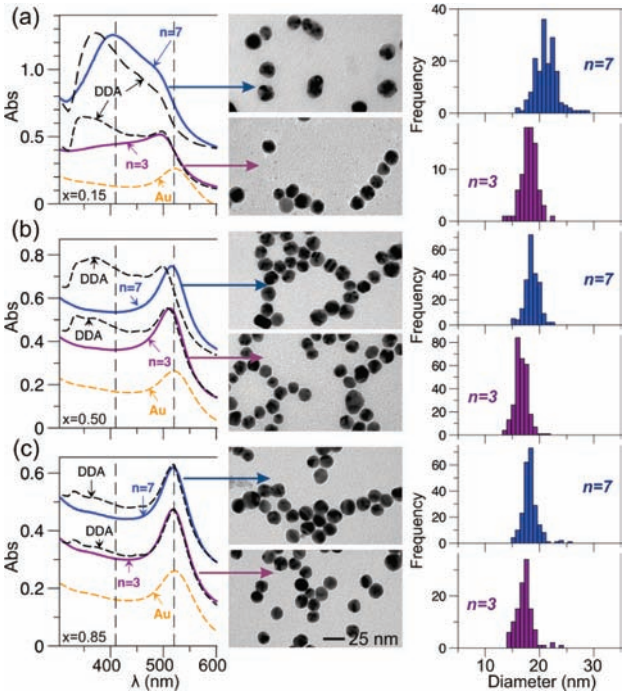

Figure 2. Optical and morphological comparisons of Au/Au_xAg_{1-x} NPs prepared at T_H = 120 °C with x = (a) 0.15, (b) 0.50, and (c) 0.85: (left) UV−vis; (middle) TEM micrographs; (right) statistical analysis comparing n = 3 and 7. UV−vis offset for clarity, identical scale bar .

We observed a unique shift in SPR as a function of shell composition (x). For example, at x = 0.50 (Figure 2b), a less dramatic blue shift was observed, with a final λ_{SPR} of ~500 nm. This λ_{SPR} was maintained despite an increase in d_{C+S} to 16.7 ± 1.8 nm (n = 3) and 18.6 ± 1.2 nm (n = 7). At x = 0.85 (Figure 2c), a nearly static λ_{SPR} of ~520 nm was observed despite the increase in d_{C+S} to 17.3 ± 1.6 nm (n = 3) and 18.3 ± 1.4 nm (n = 7). These results strongly suggest the formation of alloy shells, with more Ag-rich shells showing blue-shifted SPR. Evidence for alloy growth was further demonstrated by X-ray photoelectron spectroscopy (XPS), which showed alloy stoichiometries in agreement with the feed ratios (Table S1 in the Supporting Information).

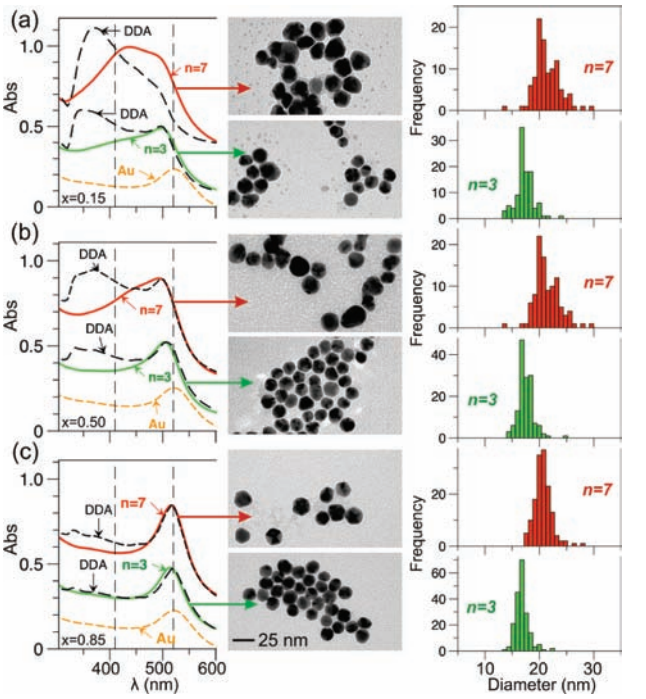

Figure 3. Optical and morphological comparisons for Au/Au_xAg_{1-x} prepared at T_H = 160 °C with x = 0.15 (a), 0.50 (b), and 0.85 (c). UV−vis (left), TEM micrographs (middle), and statistical analysis (right) comparing n = 3 and 7.

We next investigated the effect of T_H on both alloy shell growth and composition control by performing identical experiments at T_H = 160 °C (Figure 3). At T_H = 160 °C, we observed a more systematic d_{C+S} growth across the x range as well as a more thorough tailoring of λ_{SPR}. For example, at x = 0.50 (Figure 3b), we observes a new λ_{SPR} at 505 nm (n = 3) and 495 nm (n = 7). Shell growth was confirmed by TEM, which reveals d_{C+S} = 17.6 ± 1.3 and 20.4 ± 2.0 nm at n = 3 and 7 respectively. The SPR behavior was tuned to high energy at x = 0.15 (Figure 3a), and maintained at λ_{SPR} for x = 0.85 (Figure 3c).

These results show that a blue-shift in SPR is clearly possible by increasing the Ag-content in a shell of controlled thickness. However, another interesting aspect of the work is the ability to maintain the SPR characteristics of a NP at low Ag-content despite an increase in d_{C+S}. For example, Figure 3c shows the results for shell growth of composition x = 0.85 with a near constant $\lambda_{SPR} \approx$ 520 nm despite growth to d_{C+S} = 16.8 ± 1.3 (n = 3) and 20.7 ± 1.6 nm (n = 7). Alloy formation was confirmed by XPS (Table S1). This suggests that a core/alloy NP may be used to tailor the SPR energy but also to maintain a λ_{SPR} of choice independent of the NP diameter, a first such example.

Figure 4 summarizes these results by comparing d_{C+S} growth as a function of x for T_H = (a) 120 and (b) 160 °C. While both temperatures proved to be effective at tailoring the d_{C+S} increase, the NPs processed at 160 °C showed remarkably consistent values suggesting a uniform shell thickness, allowing for better comparison of SPR and alloy-shell composition. A similar comparison can be made for the tunability of λ_{SPR}, as shown in Figure 4 for (c) 120 and (d) 160 °C. For instance, at T_H = 160 °C, λ_{SPR} was found to be highly tunable on the basis of the alloy x value and d_{C+S}. It is important to note that such control of SPR is in contrast to the growth of a larger AuNP, which shows a red

dx.doi.org/10.1021/ja200650w |J. Am. Chem. Soc. 2011, 133, 5224–5227

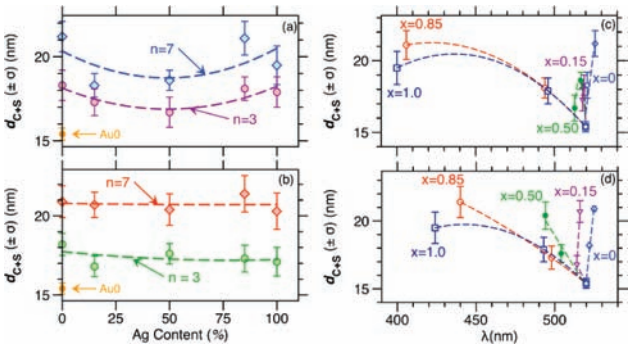

Figure 4. (a, b) Summary of the Au/Au_xAg_{1-x} d_{C+S} dependence on Ag content at T_H = (a) 120 and (b) 160 °C for n = 3 and 7. (c, d) Relationship between d_{C+S} and λ_{SPR} at T_H = (c) 120 and (d) 160 °C.

shift with increasing d_{C+S} (Figure 4, x = 0.0). Moreover, these findings suggest the ability for the most part to maintain a nearly constant λ_{SPR} for x = 0.5−0.15.

These results clearly suggest that the SPR character can be tailored by the addition of Au_xAg_{1-x} shells. To further investigate this, we compared the SPR to a model core/alloy architecture using the discrete dipole approximation method (DDA).[21] To model a core/alloy NP for the first time with DDA, we closely followed the dimensions observed using TEM by utilizing a AuNP core (d = 15.0 nm) with shells of thickness t_S = 1.0 or 3.0 nm and composition x = 0.85, 0.50, or 0.15. For this, the dielectric constant of the alloy was computed as a linear combination of the values for Ag and Au: $\varepsilon_{alloy}(x, \lambda) = x_{Ag}\varepsilon_{Ag}(\lambda) + (1 - x_{Ag})\varepsilon_{Au}(\lambda)$, where x_{Ag} is the volume fraction of Ag and ε_{Au} and ε_{Ag} are the dielectric constants for Au and Ag, respectively.[15,16] The results of the simulations are shown as dashed lines in Figure 2 and 3 with the corresponding experimental SPR. In general, the trends observed in the DDA results were closely correlated with the SPR, reinforcing the case for alloy shell growth. However, at low x values (increasing Ag content), discrepancies were observed. In particular, the differences between the SPR at T_H = 120 °C (Figure 2a) and 160 °C (Figure 3a) for n = 7 could not be modeled by this simple DDA approach. We believe the reason for this to be increased alloy interdiffusion from the core to the shell at higher T_H. For instance, the shell content would be likely to have increased x (from the core), or a thicker alloy shell would be created (core size decreases). Thus, the alloy is likely to be highly gradient in nature. Such diffusion may be enhanced by local heating at the nanoparticle interface due to the use of MWI. We are currently exploring this phenomenon in more detail.

We further utilized chemical means to decipher the core/alloy structure of the NPs. For this we employed the ligand bis-(*p*-sulfonatophenyl)phenylphosphine (BSPP). BSPP is known to oxidize Ag but not Au.[22,23] When BSPP was added at high concentration ratios ([BSPP]/[NP] > 100 000), the etching kinetics was dependent on x. Interestingly, this reaction resulted in SPR trends that are very close to the reverse of those for layer-by-layer growth (Figure S11). Figure 5 shows a temporal plot monitoring the decrease in shell SPR due to BSPP etching for samples prepared at T_H = (a) 120 and (b) 160 °C. As shown in the trends, as x increases (i.e., decreasing Ag content) the etching is less pronounced, indicating an increased alloy content of the shell itself. Such a decrease in SPR was correlated with shell etching by TEM, which revealed a decrease in d_{C+S} (Figure S10).

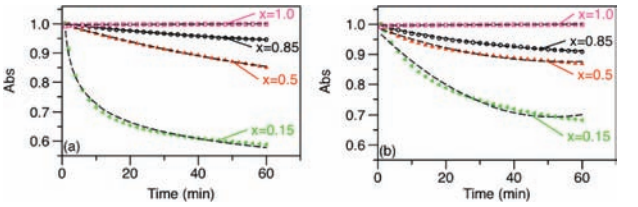

Figure 5. Summary of the results of selective Ag etching of Au/Au_xAg_{1-x}/Ag to Au/Au_xAg_{1-x} by BSPP ([BSPP]/[NP] = 100 000) for samples with x = 1, 0.85, 0.50, and 0.15 fabricated at T_H = (a) 120 and (b) 160 °C.

In summary, we have developed a new approach for processing of core/alloy NPs with optical SPR that can be tailored by both shell thickness and alloy composition. The plasmon response itself provides a valuable look into the particle ultrastructure and may provide insights into alloy interdiffusion and possible phase behavior.

■ ASSOCIATED CONTENT

Supporting Information. Figures S1−S11, Table S1, and experimental and DDA details. This material is available free of charge via the Internet at http://pubs.acs.org.

■ AUTHOR INFORMATION

Corresponding Author
mmmaye@syr.edu

■ ACKNOWLEDGMENT

We thank the Department of Chemistry and the Syracuse Biomaterials Institute (SBI) for support. This work was partially supported by a PECASE sponsored by AFOSR (FA9550-10-1-0033). We acknowledge the Cornell Center for Materials Research (CCMR NSF/DMR 0520404) for XPS and TEM access. L.H. acknowledges an NSF iREU Fellowship at SU.

■ REFERENCES

(1) Grzybowski, B. A. *Chemistry in Motion: Reaction−Diffusion Systems for Micro- and Nanotechnology*; Wiley: Chichester, U.K., 2009.
(2) (a) Ouyang, G.; Wang, C. X.; Yang, G. W. *Chem. Rev.* **2009**, *109*, 4221. (b) Detor, A. J.; Schuh, C. A. *Acta Mater.* **2007**, *55*, 4221.
(3) Luther, J. M.; Zheng, H. M.; Sadtler, B.; Alivisatos, A. P. *J. Am. Chem. Soc.* **2009**, *131*, 16851.
(4) Son, D. H.; Hughes, S. M.; Yin, Y. D.; Alivisatos, A. P. *Science* **2004**, *306*, 1009.
(5) Wark, S. E.; Hsia, C. H.; Son, D. H. *J. Am. Chem. Soc.* **2008**, *130*, 9550.
(6) Tang, X.; Tsuji, M. *CrystEngComm* **2011**, *13*, 72.
(7) Zhang, Q. B.; Xie, J. P.; Lee, J. Y.; Zhang, J. X.; Boothroyd, C. *Small* **2008**, *4*, 1067.
(8) Skrabalak, S. E.; Xia, Y. *ACS Nano* **2009**, *3*, 10.
(9) Sun, Y. G.; Xia, Y. *Nano Lett.* **2003**, *3*, 1569.
(10) Lu, X. M.; Tuan, H. Y.; Chen, J. Y.; Li, Z. Y.; Korgel, B. A.; Xia, Y. *J. Am. Chem. Soc.* **2007**, *129*, 1733.
(11) Han, H.; Di Francesco, G.; Maye, M. M. *J. Phys. Chem. C* **2010**, *114*, 19270.
(12) (a) Ferrando, R.; Jellinek, J.; Johnston, R. L. *Chem. Rev.* **2008**, *108*, 845. (b) Zhang, Q.; Xie, J.; Yu, Y.; Lee, J. Y. *Nanoscale* **2010**, *2*, 1962.

(13) (a) Gerbec, J. A.; Magana, D.; Washington, A.; Strouse, G. F. *J. Am. Chem. Soc.* **2005**, *127*, 15791. (b) Washington, A. L.; Strouse, G. F. *J. Am. Chem. Soc.* **2008**, *130*, 8916.
(14) (a) Panda, A. B.; Glaspell, G.; El-Shall, M. S. *J. Am. Chem. Soc.* **2006**, *128*, 2790. (b) Glaspell, G.; Fuoco, L.; El-Shall, M. S. *J. Phys. Chem. B* **2005**, *109*, 17350. (c) Abdelsayed, V.; Aljarash, A.; El-Shall, M. S.; Al Othman, Z. A.; Alghamdi, A. H. *Chem. Mater.* **2009**, *21*, 2825. (d) Abdelsayed, V.; Glaspell, G.; Nguyen, M.; Howe, J. M.; El-Shall, M. S. *Faraday Discuss.* **2008**, *138*, 163.
(15) Link, S.; Wang, Z. L.; El-Sayed, M. A. *J. Phys. Chem. B* **1999**, *103*, 3529.
(16) Lee, K. S.; El-Sayed, M. A. *J. Phys. Chem. B* **2005**, *109*, 20331.
(17) Link, S.; Burda, C.; Wang, Z. L.; El-Sayed, M. A. *J. Chem. Phys.* **1999**, *111*, 1255.
(18) Moores, A.; Goettmann, F. *New J. Chem.* **2006**, *30*, 1121.
(19) Mulvaney, P. *Langmuir* **1996**, *12*, 788.
(20) Hodak, J. H.; Henglein, A.; Giersig, M.; Hartland, G. V. *J. Phys. Chem. B* **2000**, *104*, 11708.
(21) Kelly, K. L.; Coronado, E.; Zhao, L. L.; Schatz, G. C. *J. Phys. Chem. B* **2003**, *107*, 668.
(22) Tan, Y. N.; Yang, J.; Lee, J. Y.; Wang, D. I. C. *J. Phys. Chem. C* **2007**, *111*, 14084.
(23) Xue, C.; Metraux, G. S.; Millstone, J. E.; Mirkin, C. A. *J. Am. Chem. Soc.* **2008**, *130*, 8337.